

LETTER TO THE EDITOR

Evidence of nuclear disks in starburst galaxies from their radial distribution of supernovae

Rubén Herrero-Illana¹, Miguel Ángel Pérez-Torres¹, and Antxon Alberdi¹

¹Instituto de Astrofísica de Andalucía - CSIC, PO Box 3004, 18008 Granada, Spain
e-mail: herrero@iaa.es

Received 01/12/2011; Accepted 12/03/2012

ABSTRACT

Galaxy-galaxy interactions are expected to be responsible for triggering massive star formation and possibly accretion onto a super-massive black hole, by providing large amounts of dense molecular gas down to the central kiloparsec region. Several scenarios to drive the gas further down to the central ~ 100 pc, have been proposed, including the formation of a nuclear disk around the black hole, where massive stars would produce supernovae. Here, we probe the radial distribution of supernovae and supernova remnants in the nuclear regions of the starburst galaxies M82, Arp 299-A, and Arp 220, by using high-angular resolution ($\lesssim 0.''1$) radio observations published in the literature (for M82 and Arp 220), or obtained by ourselves from the European VLBI Network (Arp 299-A). Our main goal was to characterize the nuclear starbursts in those galaxies and thus test scenarios that propose that nuclear disks of sizes ~ 100 pc form in the central regions of starburst galaxies. We obtained the radial distribution of supernovae (SNe) in the nuclear starbursts of M82, Arp 299-A, and Arp 220, and derived scale-length values for the putative nuclear disks powering the bursts in those central regions. The scale lengths for the (exponential) disks range from ~ 20 – 30 pc for Arp 299-A and Arp 220, up to ~ 140 pc for M82. The radial distribution of SNe for the nuclear disks in Arp 299-A and Arp 220 is also consistent with a power-law surface density profile of exponent $\gamma = 1$, as expected from detailed hydrodynamical simulations of nuclear disks. Our results support scenarios where a nuclear disk of size ~ 100 pc is formed in (U)LIRGs, and sustained by gas pressure, in which case the accretion onto the black hole could be lowered by supernova feedback.

Key words. Galaxies: starbursts – luminosity function, mass function – individual: Arp 299-A – Stars: supernovae: general – Radiation mechanisms: non-thermal – Radio continuum: stars

1. Introduction

The activity in the central regions of luminous and ultra-luminous infrared galaxies (LIRGs, $10^{11}L_{\odot} \leq L_{\text{IR}} < 10^{12}L_{\odot}$, and ULIRGs, $L_{\text{IR}} \geq 10^{12}L_{\odot}$, respectively) is powered by either accretion onto a supermassive black hole (SMBH), and/or by a burst of activity due to young, massive stars. It has been found that LIRGs and ULIRGs are associated with interacting and merging galaxies, respectively, and the interaction between the galaxies is assumed to provide large amounts of dense molecular gas that eventually reach the central regions of the galaxies, where they are responsible for triggering massive star formation and possibly accretion onto an SMBH (e.g., Di Matteo et al. 2007). While interactions and bars seem to aid the transport of the molecular gas into the kiloparsec region of galaxies (e.g., Simkin et al. 1980), it has been recognized that a major difficulty is in driving the gas from the kiloparsec region down to the central parsec, or parsecs, of (U)LIRGs, where a nuclear starburst and/or an active galactic nucleus (AGN) are expected to exist. Several mechanisms have been proposed to overcome this problem, including tidal torques driven by either stellar bars (Shlosman et al. 1990) or major and minor mergers (Mihos & Hernquist 1994, 1996), gas drag and dynamical friction in a dense nuclear star cluster (Norman & Scoville 1988), or radiation drag (Umemura 2001; Kawakatu & Umemura 2002). However, not all the accumulated gas is expected to be accreted directly onto the putative SMBH, since the removal of the angular momentum of the gas is very inefficient (Umemura 2001). The angular momentum

that is not removed will then permit the accreted gas to form a reservoir, namely a nuclear disk in the central ~ 100 pc around the AGN (e.g., Wada & Norman 2002; Kawakatu & Wada 2008, and references therein). Furthermore, if the gas in the nuclear starburst is dense enough, vigorous star formation is expected to occur, which can be detected via, e.g., high-angular resolution observations of recently exploded supernovae (e.g., in the LIRG Arp 299 (Pérez-Torres et al. 2009), or the ULIRG Arp 220 (Lonsdale et al. 2006)). The nuclear starburst is also expected to affect the growth of the SMBH, since the radiation and/or supernova (SN) feedback caused by starbursts can eventually trigger the mass accretion onto a SMBH (e.g., Umemura et al. 1997; Wada & Norman 2002).

Kawakatu & Wada (2008) proposed an scenario for (U)LIRGs, where a nuclear disk is supported by the turbulent pressure of SNe. In their model, the turbulence due to supernova activity transports the angular momentum toward the central pc-scale region. One of the implications of the model developed by Kawakatu & Wada (2008) is that the BH growth rate depends on the spatial distribution of both young stars and SNe in the nuclear disk. However, the study of this spatial distribution is a challenging observational task for two main reasons. First, the huge column densities present in nuclear starbursts cause enormous extinction towards the central regions of (U)LIRGs at optical and infrared wavelengths, such that essentially no supernova would be detected at those wavelengths in the central few hundred parsecs of a (U)LIRG. Second, the enormous angular resolution needed to discern individual objects at the

typical distances to (U)LIRGs ($\gtrsim 50$ Mpc) requires milliarcsecond angular resolution to resolve individual core-collapse supernovae (CCSNe) and/or supernova remnants (SNRs).

In this paper, we use high-angular radio observations from the literature, as well as data obtained by us, of three starburst galaxies in the local universe (M82, Arp 299-A, and Arp 220) to analyze the radial distribution of CCSNe/SNRs in their central few hundred parsecs, which may have strong implications for the (co)-evolution of AGN and (nuclear) starbursts in galaxies, in general, and in (U)LIRGs in particular.

2. The radial distribution of SNe in nuclear starbursts

The radial distribution of SNe¹ on galactic scales has been thoroughly studied (see, e.g., Bartunov et al. 1992; van den Bergh 1997; Anderson & James 2009; Hakobyan et al. 2009). Optical observations have been very useful for this purpose, as dust extinction plays a minor role in the external regions of most galaxies. However, the dust-enshrouded environments of the nuclear regions in (U)LIRGs, as well as the need for milliarcsecond angular resolution to pinpoint individual SNe, have prevented this kind of studies in the central regions of local (U)LIRGs. Fortunately, both issues –obscuration and (angular) resolution– can be overcome by means of Very Long Baseline Interferometry (VLBI) radio observations of the central regions of (U)LIRGs, since radio is dust-extinction free, and VLBI provides milliarcsecond angular resolution.

2.1. Methods

We used VLBI observations to probe the radial distribution of SNe in the nuclear regions of Arp 299-A (31 objects) and Arp 220 (48 objects), as well as MERLIN, VLA, and VLBI observations towards M82 (38 objects). For each galaxy, we fitted the surface density profile of the SNe to two different disk profiles: (i) an exponential disk, $\Sigma^{SN} = \Sigma_0^{SN} \exp(-\tilde{r}/\tilde{h}_{SN})$, and (ii) a disk with a power-law density profile with radius, $\Sigma^{SN} = \Sigma_0^{SN} (r/r_{out})^{-\gamma}$. The first case (exponential disk) assumes that the SN distribution follows the radial surface-brightness density in spiral disks (Freeman 1970), while the second one (power-law disk) was used to probe the profiles predicted by numerical simulations (Wada & Norman 2002). The notation follows the one used in Hakobyan et al. (2009), where Σ_0^{SN} is the surface density of SN at the center, \tilde{r} is the normalized radius, and r_{out} is the radius of the farthest SN analyzed, considered here to be the outer boundary of the putative nuclear disk. The main parameters that are obtained from those fits are the scale length, \tilde{h}_{SN} , and the index of the power-law profile, γ , of the putative nuclear disks in the central regions of these galaxies.

Our approach consisted in model fitting the surface density profile of the radial distribution of SNe, by determining the number of sources in concentric rings around the center of the galaxy. For this purpose, we carried out a similar data analysis to the one described in Hakobyan et al. (2009) (hereafter, H09), and we refer the reader to that paper for further details. In particular, we calculated the de-projected distance of each compact source to the center of the galaxy (the AGN, whenever its identification was possible) from the position angle of the galaxy major axis, and the inclination of the galactic disk. We obtained those parameter values from the HyperLeda database. We also

followed H09, and measured radial distances in units of R_{25} , i.e., the isophotal radius at which the surface brightness was 25 mag/arcsec² in the Johnson B filter. We then derived the surface density profile by determining the number of sources in concentric rings around the nucleus, and fitting the data to both an exponential and a power-law disk, as described above.

Since the supernova samples for all our three galaxies are of relatively small size, resulting in some small size bins, the actual uncertainties in the fits could be larger than formally obtained from a single fit. To assess the robustness of our fitting procedure, we performed a series of Monte Carlo (MC) simulations. For each galaxy, we generated 10 000 mock supernova samples, whose values were uniformly distributed within the uncertainty of each data point, and fitted them. In this way, we obtained a distribution of 10 000 different fitting values for the scale-length parameter, \tilde{h}_{SN} , and the power-law index, γ , for each galaxy. This approach allowed us to obtain more reliable values of those parameters, since no assumption was made about the Gaussianity of the distributions of both the scale length and power-law index, or of their errors. We then used the median value of the distribution of our MC values to characterize \tilde{h}_{SN} and γ , and set the uncertainty in these parameters at the 90% confidence level. To test our method, we reanalyzed the sample of H09 for 239 CCSNe within 216 host galaxies, and obtained a value of $\tilde{h}_{SN} = 0.29^{+0.02}_{-0.01}$, which is in excellent agreement with their estimate², and confirms the robustness of our analysis.

2.2. Results

We outline the results obtained for each individual galaxy. We refer the reader to the Appendices for details on the SN data used in our fitting analysis.

2.2.1. Arp 299-A

Arp 299-A ($D = 44.8$ Mpc) is one of the two interacting galaxies of the LIRG Arp 299. The sample of SNe used for our study comes from both observations from the European VLBI Network (EVN) at 5.0 GHz, presented in Pérez-Torres et al. (2009) and in Bondi et al. (2012) (see also Appendix A), as well as from published data obtained with the Very Long Baseline Array (VLBA) at 2.3 and 8.4 GHz by Ulvestad (2009). The existence and precise location of the low luminosity AGN in Arp 299-A was reported by Pérez-Torres et al. (2010), hence its position was used to calculate accurate de-projected distances for all SNe in the nuclear region of Arp 299-A. The sample has a total of 31 sources. However, although there are sources at distances as far as $\tilde{r} = 11.4 \times 10^{-2}$, only one source is further than $\tilde{r} = 6.6 \times 10^{-2}$, so the latter value of \tilde{r} was used as the limiting radius for our study, giving a final number of 30 sources. The scale length obtained using the non-linear fit is $\tilde{h}_{SN} = 1.6 \times 10^{-3}$, with a standard deviation of 0.5×10^{-3} . After performing the MC analysis, we obtained a final value \tilde{h}_{SN} of $(1.9^{+1.9}_{-0.8}) \times 10^{-3}$ and $\Sigma_0^{SN} = (1.7^{+2.8}_{-1.0}) \times 10^6$.

2.2.2. Arp 220

Arp 220 is a merging system at 77 Mpc, and the closest and most well-studied ULIRG. High-angular resolution radio ob-

² H09 report $\tilde{h}_{SN} = 0.29 \pm 0.01$. We note that the explicit list of CCSNe is not given in H09, and therefore we could not reproduce exactly their sample.

¹ In this paper, the term SNe denotes both CCSNe and SNRs.

observations from its two nuclear regions were first obtained by Lonsdale et al. (2006) using global VLBI, who found a total of 49 radio supernovae in both the east (20) and west (29) nuclei. We used the position of the peak flux density from a delay-rate VLBI map as the estimated position for the center of each galactic nucleus (Parra et al. 2007). One of the compact sources in the Arp 220 east nucleus is at a much larger distance than the rest of them, which we did not use in our fit, thus limiting the normalized radii to $\tilde{r} = 0.011$. Therefore, a total of 48 SNe were considered in the fits, which we carried both separately, for each nucleus, and for the combined data set (Fig. A.3). Similarly, we performed MC simulations for each of the two nuclei, as well as for the combined sample. In this way, we obtained a scale-length for the east and west nuclei of $(3.1^{+2.0}_{-0.7}) \times 10^{-3}$ and $(3.4^{+1.5}_{-0.9}) \times 10^{-3}$, respectively, and a combined scale-length for Arp 220 is $(3.3^{+0.6}_{-0.4}) \times 10^{-3}$. To quantify the effect of the uncertain position of the putative AGNs, we shifted them 100 times randomly around our nominal position, given by the peak flux density, by a maximum value of $\sigma_{(RA,DEC)} = \text{FWHM}/(2 \text{ S/N})$, where FWHM is the full-width at half maximum, and S/N is the signal-to-noise ratio, resulting in 4.2 mas for the east nucleus and 1.4 mas for the west one, and then fitted to the data. The maximum differences obtained were considered as a systematic error, which we added to our nominal values, such that the combined scale length became $\tilde{h}_{\text{SN}} = (3.3^{+0.7}_{-0.9}) \times 10^{-3}$, with $\Sigma_0^{SN} = (7.6^{+2.3}_{-2.1}) \times 10^5$.

2.2.3. Combination of Arp 299-A and Arp 220

The normalized radii of Arp 299-A and Arp 220 (both east and west nuclei) are comparable. We can thus combine every source prior to the analysis to obtain an average scale-length parameter with smaller errors to help characterize both nuclear starbursts. The scale length obtained for the combined samples is $\tilde{h}_{\text{SN}} = (2.0^{+0.3}_{-0.2}) \times 10^{-3}$. The original non-linear fit is shown in Fig. 1 and our MC analysis results are shown in Fig. 2. After taking into account systematic errors due to the uncertainty in the precise location of the AGNs of the Arp 220 east and west nuclei, the final value for the scale length is $\tilde{h}_{\text{SN}} = (2.0^{+0.3}_{-0.4}) \times 10^{-3}$ and $\Sigma_0^{SN} = (3.0^{+0.9}_{-0.7}) \times 10^6$.

2.2.4. M82

At a distance of 3.2 Mpc, M82 is the prototypical starburst galaxy, which has been the target of many observations at high-angular resolution. For our analysis, we combined sources catalogued as SNe (or SNR) detected by Wills et al. (1997), Allen & Kronberg (1998), McDonald et al. (2002), Fenech et al. (2008), and Brunthaler et al. (2009). These comprise observations at several frequencies with MERLIN, VLA, and VLBA, including a total of 39 sources. Since no AGN has yet been discovered in M82, we instead used the radio kinematic center of M82 (Weliachew et al. 1984) as the position of its nucleus. The scale length obtained with the MC simulation is $\tilde{h}_{\text{SN}} = (2.8^{+0.4}_{-0.3}) \times 10^{-2}$. Although the radio kinematic center is likely to be very close, if not exactly coincident, with the putative nucleus of M82, we nevertheless quantified the effect that an error in the position chosen as the nucleus of M82 would have in the fits. In particular, we shifted our fiducial position for the nucleus by up to 20 parsec in several directions, and then fitted the

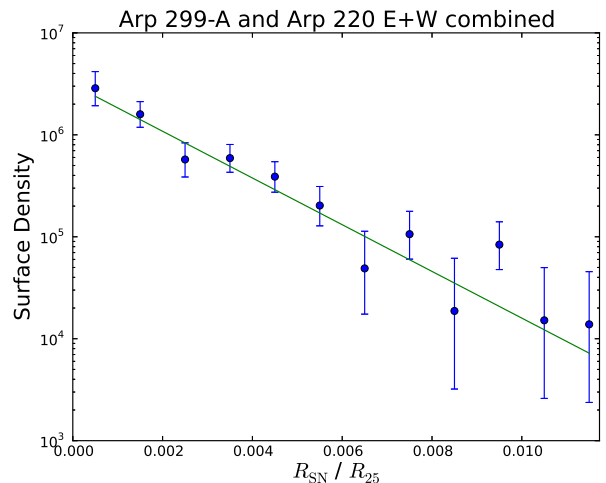


Fig. 1. Non-linear fit of the surface density profile of the combined sample of SNe from both Arp 299-A and Arp 220.

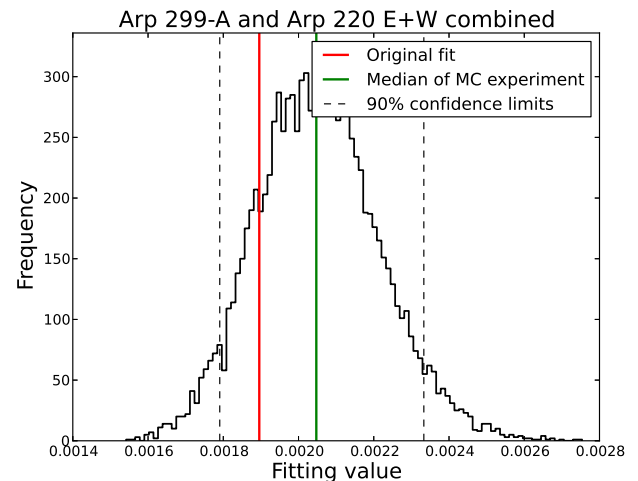


Fig. 2. MC histogram of \tilde{h}_{SN} for the combined sample of SNe from Arp 299-A and the two nuclei of Arp 220. The original non-linear fit is shown in red, and the median of the distribution created with the MC simulation is shown in green. The dashed lines correspond to the 90% confidence level interval.

data. The maximum differences were considered as a systematic error, which we added to our nominal value, thus yielding $\tilde{h}_{\text{SN}} = (2.8^{+0.9}_{-0.7}) \times 10^{-2}$, and $\Sigma_0^{SN} = (8.3^{+2.6}_{-2.3}) \times 10^3$.

3. Discussion and summary

Our main results are summarized in Table 1 and Fig. 3, where we show the scale lengths, index of the power-law SN profile, and the radial distribution of SNe for the three galaxies discussed in this paper, as well as for the sample of spiral galaxies from H09.

We note that the scale lengths for the exponential disk fits to the radial distribution of SNe in the nuclear regions of the starburst galaxies, are at least an order of magnitude smaller than those obtained by H09 for the whole disks of spiral galaxies. In particular, \tilde{h}_{SN} is two orders of magnitude smaller in the case of Arp 299-A and Arp 220. Correspondingly, the physical sizes inferred for the scale lengths of the nuclear disks (col. 3 in Table 1) are much smaller than for galactic disks: $\sim 20\text{--}30$ pc for Arp 299-

Table 1. Scale length parameters for the galaxies discussed in this paper

Nucleus	$\tilde{h}_{\text{SN}}/10^{-3}$	h_{SN} (pc)	γ
Arp 299-A	$1.9^{+1.9}_{-0.8}$	$29.3^{+29.6}_{-13.7}$	$1.1^{+0.2}_{-0.2}$
Arp 220 East	$3.1^{+2.0}_{-0.9}$	$22.2^{+14.4}_{-6.2}$	$1.0^{+0.2}_{-0.3}$
Arp 220 West	$3.4^{+1.6}_{-1.5}$	$24.4^{+11.2}_{-10.8}$	$0.8^{+0.3}_{-0.2}$
Arp 220 E+W	$3.3^{+0.7}_{-0.9}$	$23.4^{+4.7}_{-6.6}$	$0.8^{+0.1}_{-0.2}$
A299 + A220	$2.0^{+0.3}_{-0.4}$	$20.9^{+2.6}_{-2.3}$	$0.9^{+0.1}_{-0.1}$
M82	$(2.8^{+0.9}_{-0.7}) \times 10^1$	$144.4^{+21.5}_{-17.5}$	-
H09 sample	$(2.9^{+0.2}_{-0.1}) \times 10^2$	-	-

All quoted uncertainties correspond to 90% confidence limit intervals, to which a systematic error was added in the cases of Arp 220 east, Arp 220 west, and M 82, owing to the uncertainty in the precise location of their centers.

A or Arp 220, which is similar to the size derived for the nuclear starburst of the LIRG NGC 7469 (30–60 pc; Davies et al. 2004b), using CO interferometric observations, and ~ 160 pc for M82, which is also similar to the scale-length of the nuclear disk in the ULIRG/QSO Mrk 231 (Davies et al. 2004a).

We show in Fig. 3 the radial distribution of SNe in our three starburst galaxies and, for comparison, also for spiral galaxies (from the H09 sample), along with the fits to these data. We note the clear existence of three different regimes: one characterized by a very steep profile of the surface number density of SNe, which is typical of strong, nuclear starbursts (Arp 299-A+Arp 220); a second, less steep profile, as indicated for the (circum)nuclear starburst in M82; and a third, flatter profile, which is typical of very large disks, such as those in spiral galaxies (H09 sample). These results suggest that the surface density of SNe, hence of available gas to convert into stars, reaches a maximum in the vicinities of the SMBH in LIRGs and ULIRGs. We also show in col. 4 of Table 1 the fits to a power-law disk profile, consistent with the fiducial value of $\gamma = 1$ used by Wada & Norman (2002) and Kawakatu & Wada (2008) for the nuclear disk, and appears to yield further support to their modeling.

We have modeled for the first time the radial distribution of SNe in the nuclear starbursts of M82, Arp 299-A, and Arp 220, and derived scale-length values for exponential disks, which are in the range between ~ 20 pc and ~ 140 pc. We have also modeled these SNe distributions as power-law disk profiles, and found that they agree with state-of-the-art numerical simulations of nuclear disks around SMBHs. We interpret our results as evidence of nuclear disks around the centers, i.e., AGNs, of starburst-dominated galaxies and also support for evolutionary scenarios where a nuclear disk of size $\lesssim 100$ pc is formed in LIRGs and ULIRGs (Kawakatu & Wada 2008). In particular, the scale-length obtained for the LIRG Arp 299-A and the LLAGN nature of its SMBH (Pérez-Torres et al. 2010), suggests that its nuclear disk is likely supported by gas pressure, such that the accretion onto the SMBH is smaller than for a turbulent-supported disk. It is very likely that this is also the case for the ULIRG Arp 220. Future deep VLBI observations of a significantly large sample of (U)LIRGs, which would result in the discovery of new SN factories, will be of much use for deriving statistically significant results on the size of nuclear disks, and thus setting useful constraints on (co)-evolutionary scenarios.

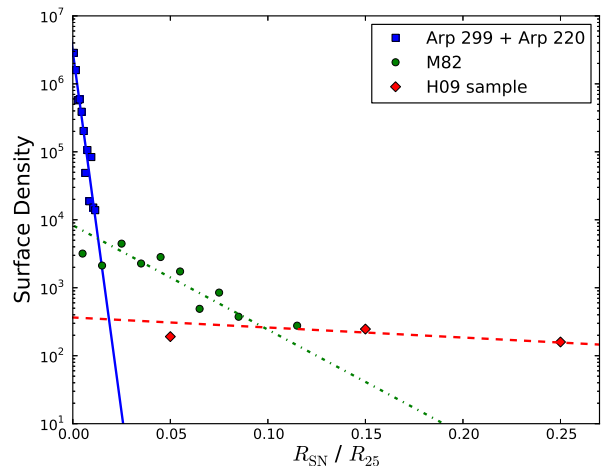


Fig. 3. Radial distribution of SNe for (nuclear) starbursts and spiral galaxies. The data correspond to the combined Arp 299-A + Arp 220 sample (blue squares), M82 (green circles), and the H09 sample of spiral galaxies (red diamonds), and the fitted lines are for Arp 299-A + Arp 220 (solid line), M82 (dotted-dashed line), and H09 (dashed line). For the sake of clarity, only the innermost part of the H09 sample is shown in the plot.

Acknowledgements. We are grateful to Rob Beswick and the anonymous referee for useful suggestions and comments. The authors acknowledge support by the Spanish MICINN through grant AYA2009-13036-CO2-01, partially funded by FEDER funds. This research has also been partially funded by the Autonomic Government of Andalusia under grants P08-TIC-4075 and TIC-126. We acknowledge the usage of the HyperLeda database (<http://leda.univ-lyon1.fr/>).

References

- Allen, M. L. & Kronberg, P. P. 1998, *ApJ*, 502, 218
 Anderson, J. P. & James, P. A. 2009, *MNRAS*, 399, 559
 Bartunov, O. S., Makarova, I. N., & Tsvetkov, D. I. 1992, *A&A*, 264, 428
 Bondi, M., Pérez-Torres, M. A., Herrero-Illana, R., & Alberdi, A. 2012, *ArXiv*
 Brunthaler, A., Menten, K. M., Reid, M. J., et al. 2009, *A&A*, 499, L17
 Davies, R. I., Tacconi, L. J., & Genzel, R. 2004a, *ApJ*, 613, 781
 Davies, R. I., Tacconi, L. J., & Genzel, R. 2004b, *ApJ*, 602, 148
 Di Matteo, P., Combes, F., Melchior, A.-L., & Semelin, B. 2007, *A&A*, 468, 61
 Fenech, D. M., Muxlow, T. W. B., Beswick, R. J., Pedlar, A., & Argo, M. K. 2008, *MNRAS*, 391, 1384
 Freeman, K. C. 1970, *ApJ*, 160, 811
 Hakobyan, A. A., Mamon, G. A., Petrosian, A. R., Kunth, D., & Turatto, M. 2009, *A&A*, 508, 1259
 Kawakatu, N. & Umemura, M. 2002, *MNRAS*, 329, 572
 Kawakatu, N. & Wada, K. 2008, *ApJ*, 681, 73
 Lonsdale, C. J., Diamond, P. J., Thrall, H., Smith, H. E., & Lonsdale, C. J. 2006, *ApJ*, 647, 185
 McDonald, A. R., Muxlow, T. W. B., Wills, K. A., Pedlar, A., & Beswick, R. J. 2002, *MNRAS*, 334, 912
 Mihos, J. C. & Hernquist, L. 1994, *ApJ*, 425, L13
 Mihos, J. C. & Hernquist, L. 1996, *ApJ*, 464, 641
 Norman, C. & Scoville, N. 1988, *ApJ*, 332, 124
 Parra, R., Conway, J. E., Diamond, P. J., et al. 2007, *ApJ*, 659, 314
 Pérez-Torres, M. A., Alberdi, A., Romero-Cañizales, C., & Bondi, M. 2010, *A&A*, 519, L5+
 Pérez-Torres, M. A., Romero-Cañizales, C., Alberdi, A., & Polatidis, A. 2009, *A&A*, 507, L17
 Portegies Zwart, S. F., McMillan, S. L. W., & Gieles, M. 2010, *ARA&A*, 48, 431
 Shlosman, I., Begelman, M. C., & Frank, J. 1990, *Nature*, 345, 679
 Simkin, S. M., Su, H. J., & Schwarz, M. P. 1980, *ApJ*, 237, 404
 Ulvestad, J. S. 2009, *AJ*, 138, 1529
 Umemura, M. 2001, *ApJ*, 560, L29
 Umemura, M., Fukue, J., & Mineshige, S. 1997, *ApJ*, 479, L97
 van den Bergh, S. 1997, *AJ*, 113, 197
 Wada, K. & Norman, C. A. 2002, *ApJ*, 566, L21

- Weliachew, L., Fomalont, E. B., & Greisen, E. W. 1984, *A&A*, 137, 335
Wills, K. A., Pedlar, A., Muxlow, T. W. B., & Wilkinson, P. N. 1997, *MNRAS*, 291, 517

Appendix A: Arp 299-A and Arp 220
Table A.1. Arp 299-A^a source list

Name	$\Delta \alpha^b$ (J2000.0)	$\Delta \delta$ (J2000.0)	Deprojected dist. (mas)
A3	33.5941	46.560	252.3
A15	33.5991	46.637	190.9
33.612+46.70 ^c	33.6124	46.696	71.3
33.615+46.67 ^c	33.6154	46.667	47.9
A26	33.6163	46.652	55.6
33.617+46.72 ^c	33.6173	46.724	44.2
A18	33.6195	46.463	276.6
A19	33.6198	46.660	45.1
A6	33.6207	46.597	122.6
A0	33.6212	46.707	13.2
A2	33.6218	46.655	60.5
A27	33.6221	46.692	25.06
33.624+46.77 ^c	33.6241	46.771	81.9
33.627+46.44 ^c	33.6267	46.440	331.2
A28	33.6272	46.719	66.8
33.628+46.62 ^c	33.6280	46.623	135.8
33.629+46.65 ^c	33.6290	46.647	121.6
A7	33.6301	46.786	117.7
A8	33.6305	46.401	394.6
A9	33.6307	46.620	159.4
A29	33.6344	46.915	249.6
A22	33.6355	46.677	160.6
A30	33.6362	46.863	209.1
A10	33.6392	46.551	291.6
A11	33.6403	46.582	272.9
A31	33.6441	46.629	271.1
A12	33.6495	46.590	347.3
A4	33.6500	46.537	394.0
A25	33.6523	46.701	311.8
A13	33.6531	46.733	309.6
A14	33.6825	46.570	666.2

^a Arp 299-A has a major axis position angle of $PA = 163.6^\circ$ and an inclination of its galactic disk of $i = 52.4^\circ$.

^b Coordinates are given with respect to $\alpha(J2000.0) = 11:28:00.0000$ and $\delta(J2000.0) = 58:33:00.000$, (see Bondi et al. 2012).

^c Sources from Ulvestad (2009).

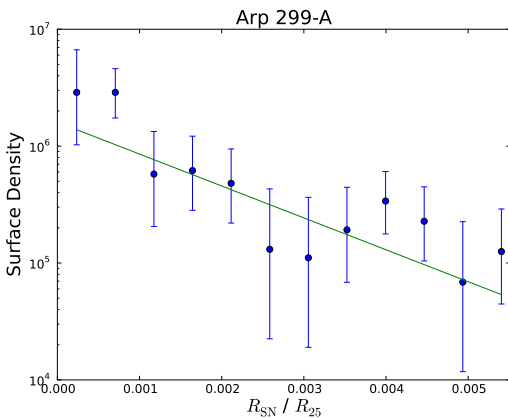


Fig. A.1. Surface density profile of the 30 inner SNe in Arp 299-A. The solid green line is a non-linear fit to an exponential disk with $\tilde{h}_{SN} = 1.6 \times 10^{-3}$ and $\Sigma_0^{SN} = 1.6 \times 10^6$.

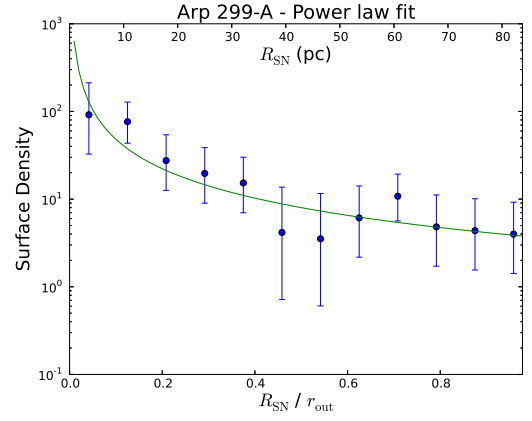


Fig. A.2. Surface density of SNe vs radii normalized to the furthest source, r_{out} , in Arp 299-A and non-linear fit to a power law with $\gamma = 1.1$.

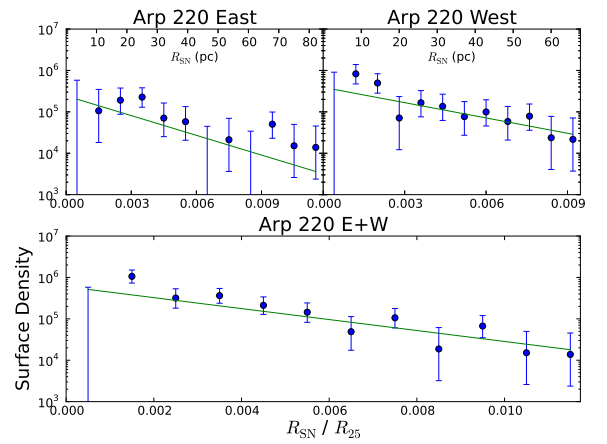


Fig. A.3. Non-linear fits to the surface density profile of the radial distribution of SNe in Arp 220. *Top left:* Fit to the 19 inner sources in the eastern nucleus ($\tilde{h}_{SN} = 2.7 \times 10^{-3}$). *Top right:* Fit to the 29 sources in the western nucleus ($\tilde{h}_{SN} = 3.5 \times 10^{-3}$). *Bottom:* Combined fit for the SNe in the east and west nuclei (48 sources), yielding $\tilde{h}_{SN} = 3.3 \times 10^{-3}$ and $\Sigma_0^{SN} = 6.0 \times 10^5$. We note that some of the points are in rings where no sources were detected. While their corresponding surface density is zero, their upper limits were used in the fit.

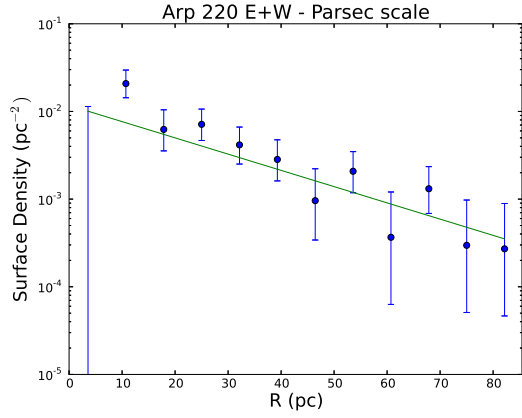


Fig. A.4. Surface density profile of the combined sources for the east and west nuclei of Arp 220, in parsecs. The non-linear fit yields a scale length of $h_{\text{SN}} = 23.4$ pc, with $\Sigma_0^{\text{SN}} = 1.2 \times 10^{-2} \text{ pc}^{-2}$.

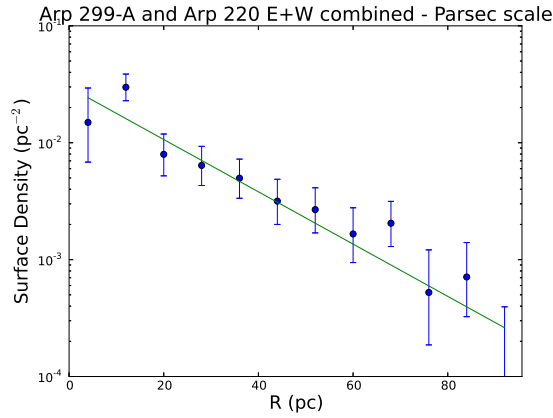


Fig. A.5. Surface density profile of the combined sources for Arp 299-A and Arp 220, in parsecs. The non-linear fit yields a scale-length of $h_{\text{SN}} = 19.4$ pc and $\Sigma_0^{\text{SN}} = 3.0 \times 10^{-2} \text{ pc}^{-2}$.

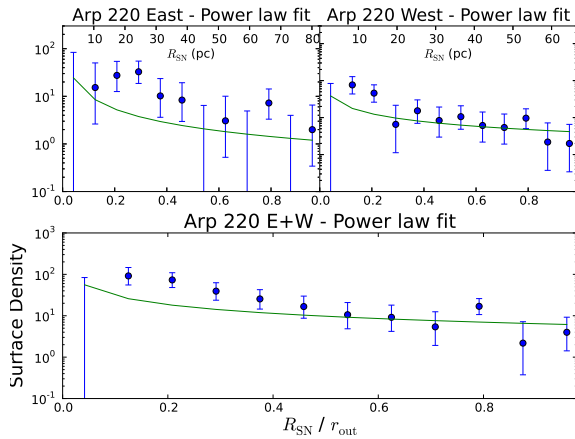


Fig. A.6. Non-linear power-law fits of the surface density of SNe vs radius, normalized to the furthest source, r_{out} , in Arp 220. *Top left:* East nucleus, with $\gamma = 1.0$. *Top right:* West nucleus, with $\gamma = 0.7$. *Bottom:* Combined analysis for the East and West nuclei (48 sources), yielding $\gamma = 0.7$. Note that some of the points are in rings where no sources were detected. While their corresponding surface density is zero, their upper limits were used in the fit.

Table A.2. Arp 220^a source list

Name	$\Delta \alpha^b$ (J2000.0)	$\Delta \delta$ (J2000.0)	Deprojected dist. (mas)
W46	57.2066	11.459	310.4
W44	57.2082	11.548	254.8
W42	57.2123	11.482	215.6
W41	57.2161	11.405	264.9
W40	57.2162	11.478	167.4
W39	57.2171	11.484	150.3
W34	57.2195	11.492	112.1
W33	57.2200	11.492	106.0
W30	57.2211	11.398	235.7
W29	57.2212	11.445	157.1
W28	57.2212	11.541	82.8
W27	57.2219	11.387	251.9
W26	57.2223	11.435	164.4
W25	57.2223	11.500	69.0
W24	57.2224	11.514	58.1
W19	57.2240	11.499	48.9
W18	57.2240	11.546	62.8
W17	57.2241	11.520	34.3
W16	57.2244	11.531	39.7
W15	57.2253	11.483	62.4
W14	57.2270	11.573	107.1
W12	57.2295	11.524	47.1
W11	57.2300	11.503	50.0
W10	57.2306	11.502	57.8
W09	57.2318	11.401	209.3
W08	57.2360	11.431	186.6
W07	57.2362	11.547	154.4
W03	57.2387	11.401	248.7
E22	57.2758	11.277	169.3
E21	57.2789	11.293	127.4
E20	57.2821	11.185	189.2
E19	57.2840	11.151	235.3
E18	57.2843	11.226	104.8
E17	57.2850	11.193	156.5
E16	57.2848	11.472	361.0
E14	57.2868	11.297	46.8
E13	57.2878	11.308	66.3
E12	57.2885	11.212	109.5
E11	57.2910	11.325	111.7
E10	57.2914	11.332	126.4
E09	57.2915	11.477	384.8
E08	57.2931	11.328	132.9
E07	57.2943	11.279	90.5
E06	57.2946	11.264	91.2
E05	57.2980	11.419	319.7
E04	57.2986	11.408	306.3
E03	57.3073	11.333	305.8
E01	57.3103	11.577	676.1

^a Arp 220 has an inclination angle of 57.0° , with a major-axis position angle of 96.5° .

^b Coordinates are given with respect to $\alpha(\text{J2000.0}) = 15:34:00.0000$ and $\delta(\text{J2000.0}) = 23:30:00.000$.

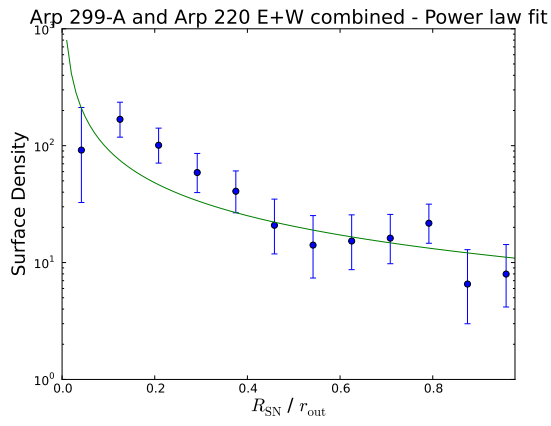


Fig. A.7. Surface density of SNe vs radii normalized to the furthest source, r_{out} , for the combined sample of SNe from Arp 299-A and the two nuclei of Arp 220. A non-linear fit to a power law with radius yields $\gamma = 0.9$.

Appendix B: M82

Table B.1. M82^a source list

Name ^b	$\Delta \alpha^c$ (J2000.0)	$\Delta \delta$ (J2000.0)	Deprojected dist. (mas)
39.10+57.3	47.87	43.74	37.03
39.40+56.2	48.16	42.53	29.20
39.64+53.3	48.41	39.68	20.00
39.77+56.9	48.54	43.36	27.84
40.32+55.2	49.07	41.53	16.98
40.61+56.3	49.32	42.19	15.93
40.68+55.1	49.42	41.42	14.13
41.30+59.6	50.05	45.92	20.40
41.95+57.5	50.70	44.00	6.94
42.61+60.7	51.35	46.89	9.35
42.66+51.6	51.38	47.76	13.21
42.67+55.6	51.37	41.78	17.44
42.67+56.3	51.40	42.65	13.42
42.80+61.2	51.54	47.53	10.25
43.18+58.2	51.91	44.58	8.70
43.31+59.2	52.03	45.42	5.75
43.40+62.6	52.11	48.74	10.22
43.55+60.0	52.27	46.31	4.22
43.72+62.6	52.43	48.79	7.63
43.82+62.8	52.54	48.98	7.71
44.01+59.6	52.72	45.77	12.03
44.08+63.1	52.75	49.46	8.50
44.28+59.3	52.99	45.53	16.33
44.34+57.8	53.05	43.94	24.65
44.40+61.8	53.13	47.87	8.35
44.51+58.2	53.22	44.36	24.59
44.89+61.2	53.61	47.35	15.69
45.17+61.2	53.88	47.41	18.61
45.24+65.2	53.96	51.36	12.15
45.42+67.4	54.13	53.53	18.13
45.52+64.7	54.22	50.94	12.94
45.75+65.3	54.44	51.43	14.17
45.79+64.0	54.50	50.22	16.24
45.89+63.8	54.60	49.98	17.85
46.52+63.9	55.21	50.05	24.19
46.56+73.8	55.26	59.90	38.39
46.70+67.1	55.41	53.16	19.71
47.37+68.0	56.10	54.00	24.01
SN2008iz	51.55	45.79	2.41

^a M82 has a major position angle of 67.5° and an inclination of 79.4° .

^b Names from the literature are derived from B1950 coordinates.

^c Coordinates are given with respect to $\alpha(\text{J2000.0}) = 09:55:00.00$ and $\delta(\text{J2000.0}) = 69:40:00.00$.

Appendix C: Nature of the radio sources

The sources used in this paper are classified generically as supernovae (SNe), by which we mean core collapse supernovae (CCSNe) and supernova remnants (SNR). In the case of M82, the closest of the three galaxies discussed here, we used the source list in McDonald et al. (2002) and Fenech et al. (2008), where the authors already discriminate SNe from HII regions based on their spectral shape, brightness temperature, and observed shell structure. In the cases of the more distant galaxies, Arp 299 and Arp 220, we used available spectral information from the literature, and especially, the brightness temperatures inferred from VLBI observations, which for

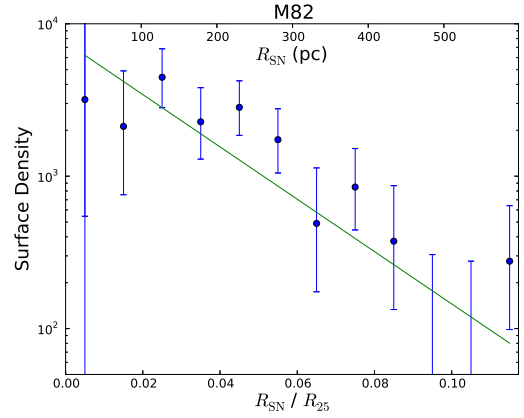


Fig. B.1. Surface density profile for the radial distribution of SNe in M82 (39 objects). The solid green line is a non-linear fit to an exponential disk with $\tilde{h}_{\text{SN}} = 2.5 \times 10^{-2}$ and $\Sigma_0^{\text{SN}} = 7.5 \times 10^3$.

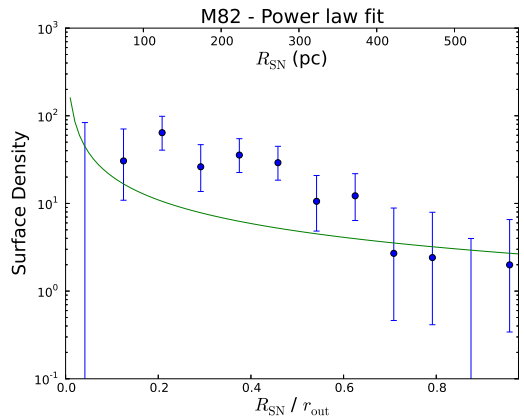


Fig. B.2. Surface density of SNe vs radii normalized to the furthest source, r_{out} and non-linear fit to a power law (nuclear) disk for M82. The poor goodness of the fit does not seem to be consistent with a nuclear disk whose SN surface density follows a power law in the central few hundred pc.

all of the sources correspond to non-thermal radio emitters (e.g., Pérez-Torres et al. (2009) for Arp 299A, Parra et al. (2007) for Arp 220).

Single or multiple ultra compact HII (UC HII) regions can be ruled out because their ionizing radiation is normally dominated by a single O star, whose maximum free-free thermal radio luminosity is several orders of magnitude below the radio luminosity from any of the objects detected in either Arp 299-A or Arp 220. The expected thermal radio emission from super star clusters (SSCs), which can host up to a few 10^5 stars, similarly cannot be responsible for the observed emission. At the distances of Arp 299 and Arp 220, the VLBI beam sizes correspond to ~ 1.5 pc, implying radial sizes of at most about 0.8 pc. Young massive stellar clusters of this size have a mass of at most $5 \times 10^5 M_\odot$ (e.g. Portegies Zwart et al. 2010). Assuming a Kroupa initial mass function with $\alpha = -1.0$ between 0.1 and $0.5 M_\odot$, and $\alpha = -2.35$ between 0.5 and $100 M_\odot$, the number of O6 and earlier type stars is 142 (out of a total of 10^5 stars), hence the maximum attainable thermal radio luminosity would be $\sim 2 \times 10^{25}$ erg/s/Hz, which is at least an order of magnitude lower than observed in Arp 299-A or Arp 220.